

## Supplementary Materials for

### Real-time tracking of fluorescent magnetic spore-based microrobots for remote detection of *C. diff* toxins

Yabin Zhang, Lin Zhang, Lidong Yang, Chi Ian Vong, Kai Fung Chan, William K. K. Wu, Thomas N. Y. Kwong, Norman W. S. Lo, Margaret Ip, Sunny H. Wong, Joseph J. Y. Sung, Philip W. Y. Chiu, Li Zhang\*

\*Corresponding author. Email: lizhang@mae.cuhk.edu.hk

Published 11 January 2019, *Sci. Adv.* 5, eaau9650 (2019)  
DOI: 10.1126/sciadv.aau9650

#### The PDF file includes:

- Fig. S1. Cross-section SEM images of the prepared samples.
- Fig. S2. Magnetization curves of the prepared samples.
- Fig. S3. Optical properties of the prepared samples.
- Fig. S4. Magnetization direction of multiple FMSMs and single FMSM.
- Fig. S5. Motion trajectories of an FMSM in various media over 5-s time frames.
- Fig. S6. Optical images of the FMSMs under different illuminations.
- Fig. S7. Fluorescence time-lapse images of static and moving FMSMs in bacterial supernatants.
- Fig. S8. MSD of the microtracers caused by the motion of the FMSMs.
- Fig. S9. Fluorescence responses of the FMSMs toward different substances.
- Fig. S10. The survey results of the alignment of CROP segment of *C. diff* toxin B (amino acids 1830 to 2366) using Smart BLAST provided by the National Center for Biotechnology Information online.
- Fig. S11. Schematic for the structures of *C. diff* toxins and mechanism of quenching by the CROP segment of *C. diff* toxins to CDs on the FMSMs.
- Fig. S12. Fluorescence changes in different motion modes.
- Fig. S13. Detection calibration curves of the FMSMs.
- Fig. S14. Future automated control detection strategy.
- Table S1. Specific surface areas and pore parameters of the samples.
- Legends for movies S1 to S5

#### Other Supplementary Material for this manuscript includes the following:

(available at [advances.sciencemag.org/cgi/content/full/5/1/eaau9650/DC1](https://advances.sciencemag.org/cgi/content/full/5/1/eaau9650/DC1))

- Movie S1 (.mp4 format). Magnetic actuation of the FMSMs using a rotating magnetic field.
- Movie S2 (.mp4 format). Swimming of the FMSMs in different media.
- Movie S3 (.mp4 format). Fluorescence tracking of the FMSMs in different media.

Movie S4 (.mp4 format). Automated fluorescence signal-based servoing of the FMSMs in predefined trajectories.

Movie S5 (.mp4 format). Fluorescence detection using the FMSMs in clinical stool supernatant.

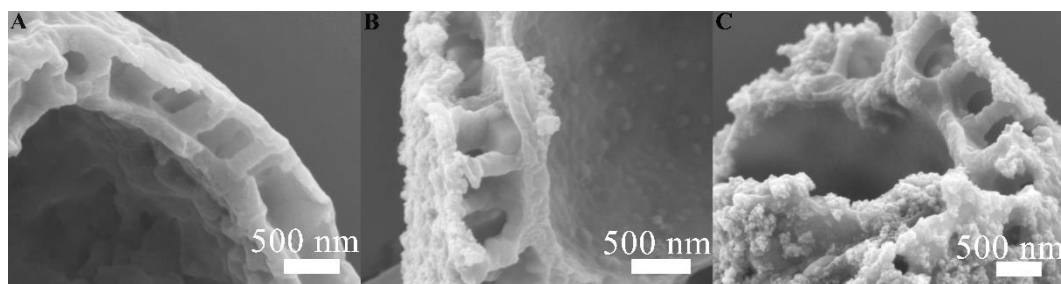


**Fig. S1. Cross-section SEM images of the prepared samples.** (A) Original spore, (B) spore@Fe<sub>3</sub>O<sub>4</sub> hybrid and (C) fluorescent magnetic spore-based (spore@Fe<sub>3</sub>O<sub>4</sub>@CDs) microrobot (FMSM).

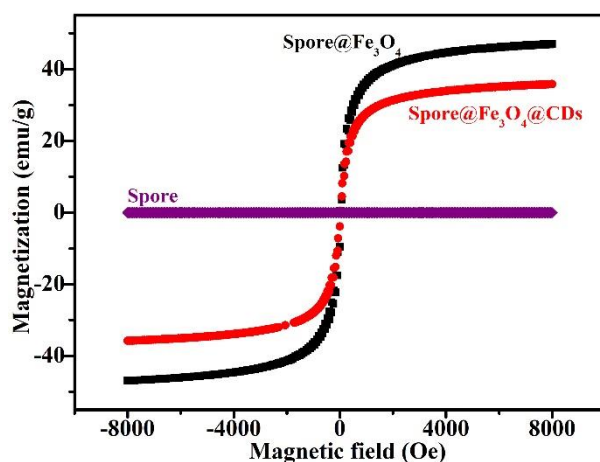


**Fig. S2. Magnetization curves of the prepared samples.** (Original spores, spore@Fe<sub>3</sub>O<sub>4</sub> hybrids and the FMSMs.)

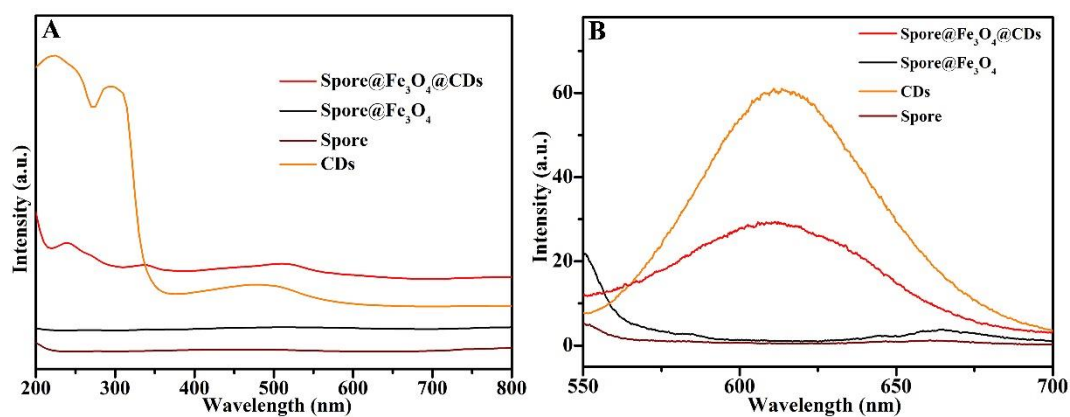


**Fig. S3. Optical properties of the prepared samples.** (A) UV-Vis and (B) fluorescence spectra of original spores, carbon dots, spore@Fe<sub>3</sub>O<sub>4</sub> hybrids and the FMSMs.

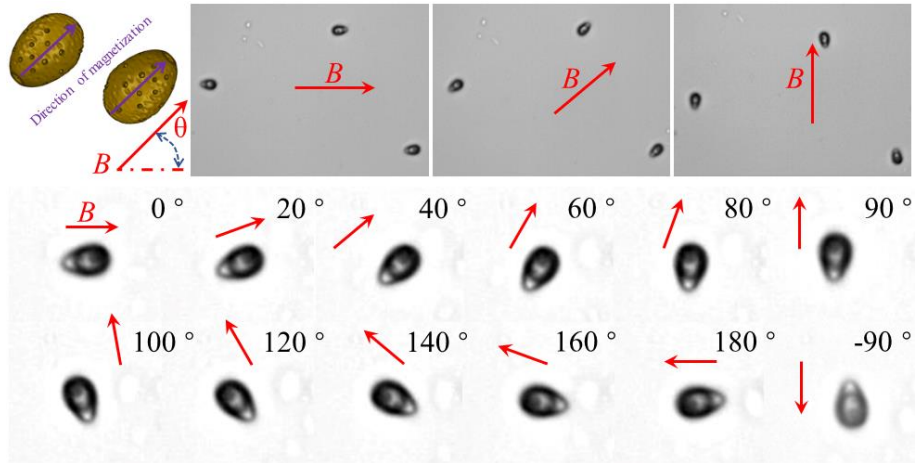


**Fig. S4. Magnetization direction of multiple FMSMs and single FMSM.** When placed in the magnetic field with different orientations (red arrows), the FMSMs can be magnetized along their long axis of droplet-like morphology (purple arrows) due to the encapsulation of  $\text{Fe}_3\text{O}_4$  nanoparticles.

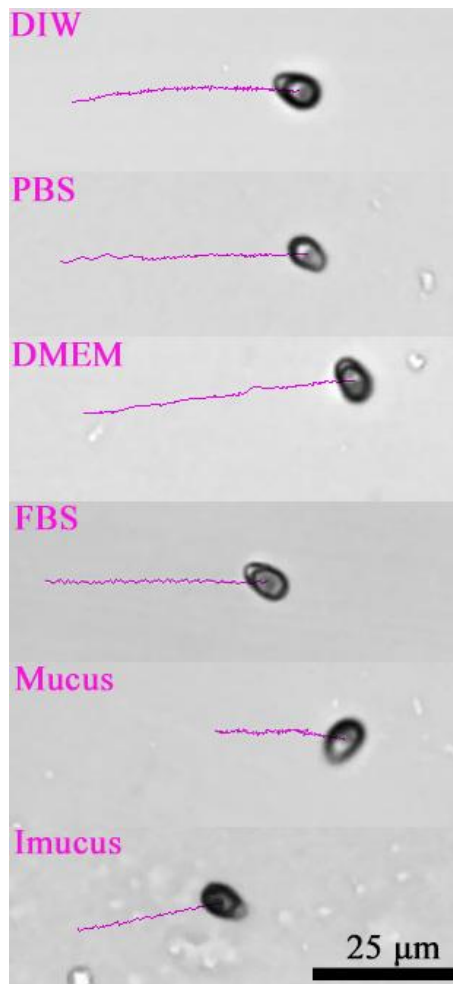


**Fig. S5. Motion trajectories of an FMSM in various media over 5-s time frames.** (A) Deionized water (DIW), (B) phosphate buffered saline (PBS), (C) Dulbecco's modified Eagle's medium (DMEM), (D) fetal bovine serum (FBS), (E) mucus from pig stomachs, (F) intestinal mucus (Imucus) from pig guts.

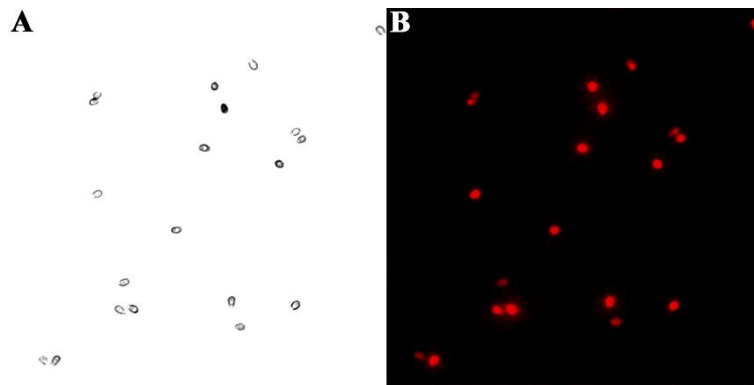


**Fig. S6. Optical images of the FMSMs under different illuminations.** (A) Under the illumination of white light and (B) the green light excitation (excitation filter: 537-552 nm, emission filter: 582-637 nm).

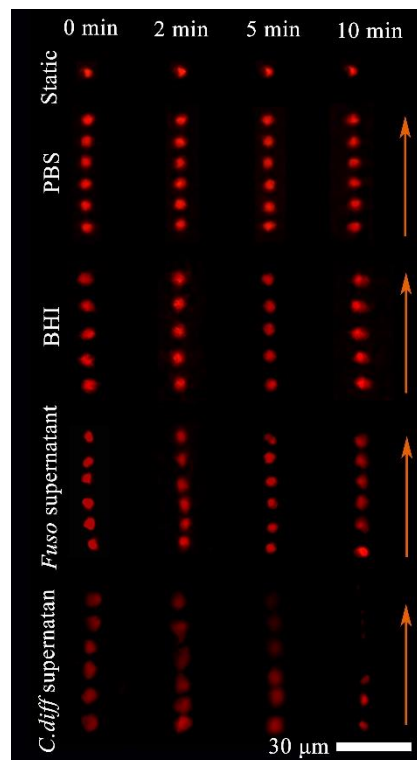


**Fig. S7. Fluorescence time-lapse images of static and moving FMSMs in bacterial supernatants.** In different tested samples and at different moving time.

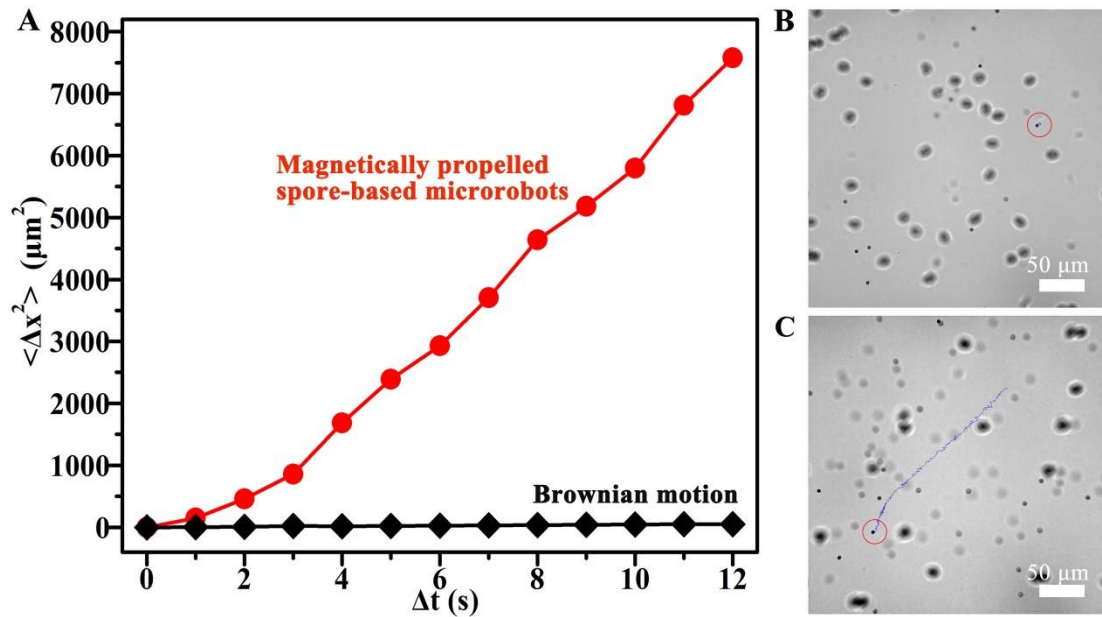


**Fig. S8. MSD of the microtracers caused by the motion of the FMSMs.** (A) Mean-squared displacement *versus* time interval obtained by averaging over 12 passive PS beads with a diameter of 3  $\mu\text{m}$ . Their trajectories are affected by active FMSMs swimming for 12 s in water, compared with that governed only by Brownian motion upon time. The right images show the typical tracking trajectories (blue lines) of PS tracers (enclosed by red circles) undergoing Brownian motion (B) and a synergic effect of Brownian motion and convection produced by motile FMSMs (C) in water.

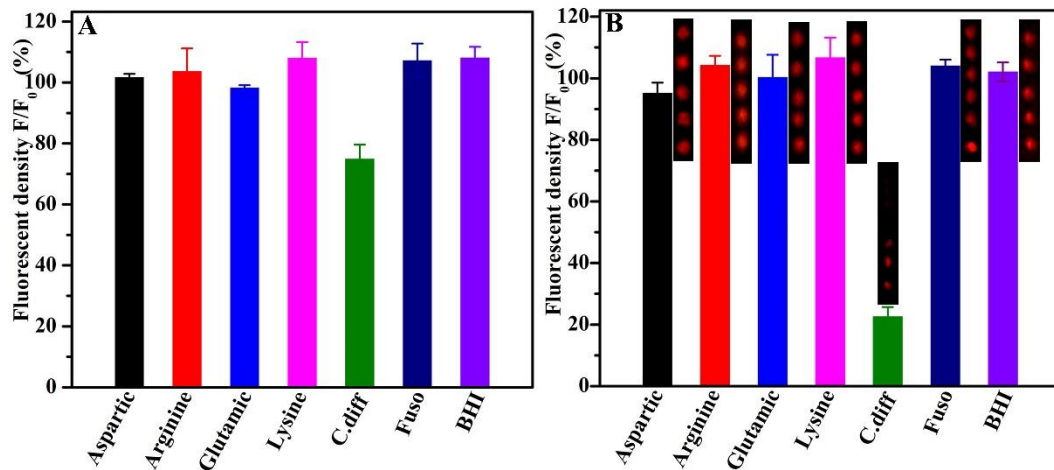


**Fig. S9. Fluorescence responses of the FMSMs toward different substances.** Fluorescence intensity of (A) static FMSMs staying for 30 min and (B) mobile FMSMs navigating for 10 min in the presence of an excess concentration (10 mg/mL) of aspartic acid, arginine acid, glutamic and lysine as well as the same concentration (0.1C,  $C=37.60$  ng/mL) of *Fuso* bacteria supernatant and BHI. Insets show fluorescent time-lapse images with the upward motion.

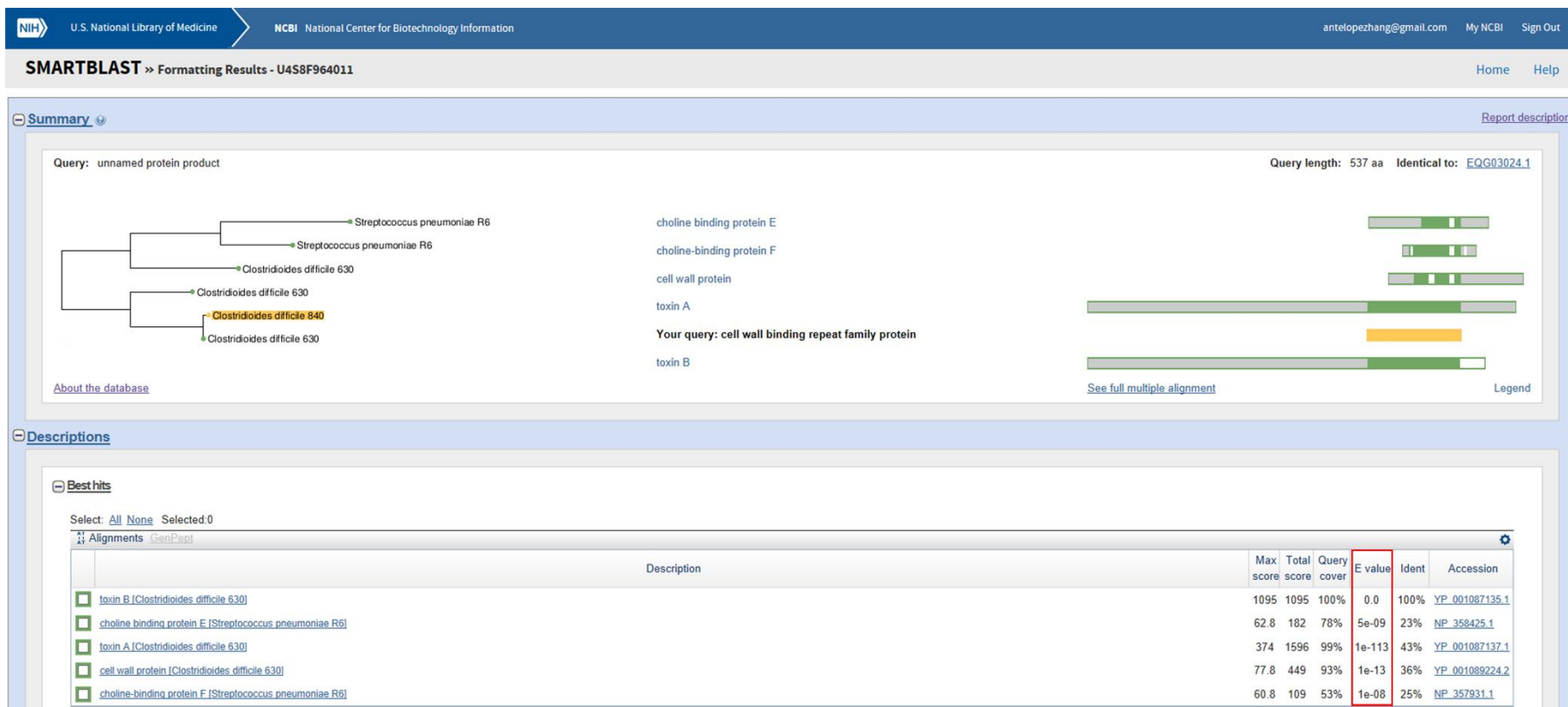


**Fig. S10. The survey results of the alignment of CROP segment of *C. diff* toxin B (amino acids 1830 to 2366) using Smart BLAST provided by the National Center for Biotechnology Information online.** A concise summary of the matches (five best ones) from well-studied reference species shows phylogenetic relationships, a schematic diagram form of the alignment coverage and conserved protein domains identified. The specific descriptions are given to list the matches in “Best hits” table from the landmark dataset or the non-redundant protein database (NR) and “Additional BLAST Hits” table from NR and the reference dataset. The detailed alignments between the query and matched database sequences are provided in Alignment section (Refer to webpage: <https://blast.ncbi.nlm.nih.gov/smartblast/smartBlast.cgi>). Based on these matching results and the corresponding analyses, we concluded that

the alignment of CROPs segment of *C. diff* toxin B (amino acids:1830-2366) does share high homology (93%-99%) with cell wall protein and toxin A of *Clostridiodes difficile* as well as moderate homology (53-78%) with cholin-binding proteins E/F which only exist in bacterium *Streptococcus pneumoniae*. As we know, matched database sequences with E-values less than  $10^{-4}$  (enclosed by red rectangle) can be considered preferentially to be homologous or related to the sequence of CROPs segment. Moreover, the smaller the E-value is, the higher the similarity will be. Thus, it is speculated that the highly similar sequences to CROPs segment can be found only in toxin A/toxin B of *Clostridiodes difficile* and cholin-binding proteins E/F of *Streptococcus pneumoniae*. Nevertheless, it is found that *Streptococcus pneumoniae* should be existed in respiratory tract instead of gastrointestinal tract (GI), which would have no influence on the detection of *C. diff* toxins from GI. These formatting results demonstrate that the FMSMs are not able to target the toxins secreted by other bacteria in GI due to the absence of CROPs in their receptor-binding domains, excluding the possibility of false positives from the interference of other toxins and bacteria in real samples and demonstrating the specificity of targeting *C. diff* toxins.

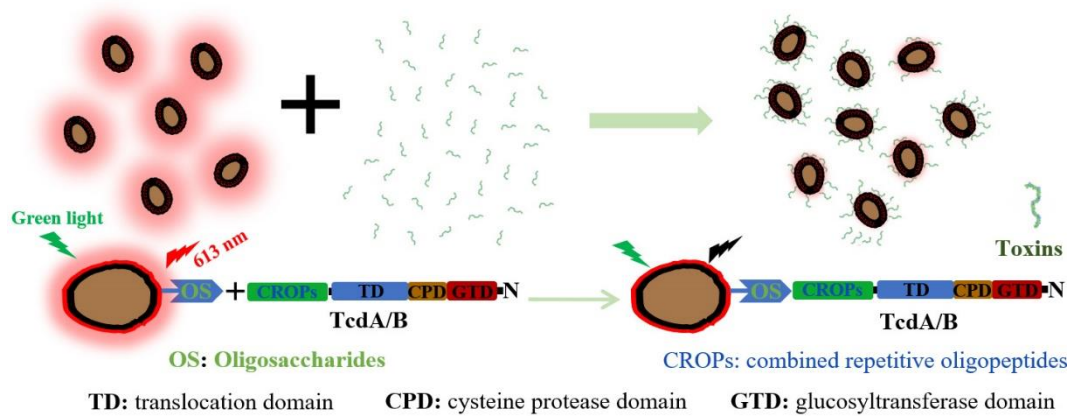


**Fig. S11. Schematic for the structures of *C. diff* toxins and mechanism of quenching by the CROP segment of *C. diff* toxins to CDs on the FMSMs.**

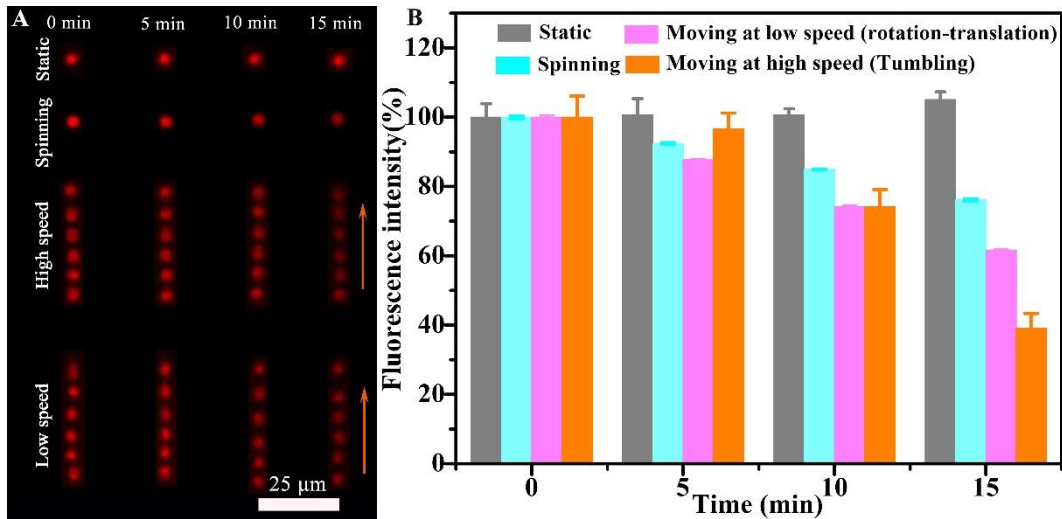


**Fig. S12. Fluorescence changes in different motion modes. (A)** Fluorescent time-lapse images of single static, spinning, slowly and rapidly moving FMSM in 0.1C ( $C=8.66$  ng/mL) clinical stool supernatant. **(B)** The changing trend of the fluorescence intensity of single static, spinning, slowly and rapidly moving FMSM navigated for different time in 0.1C stool samples.

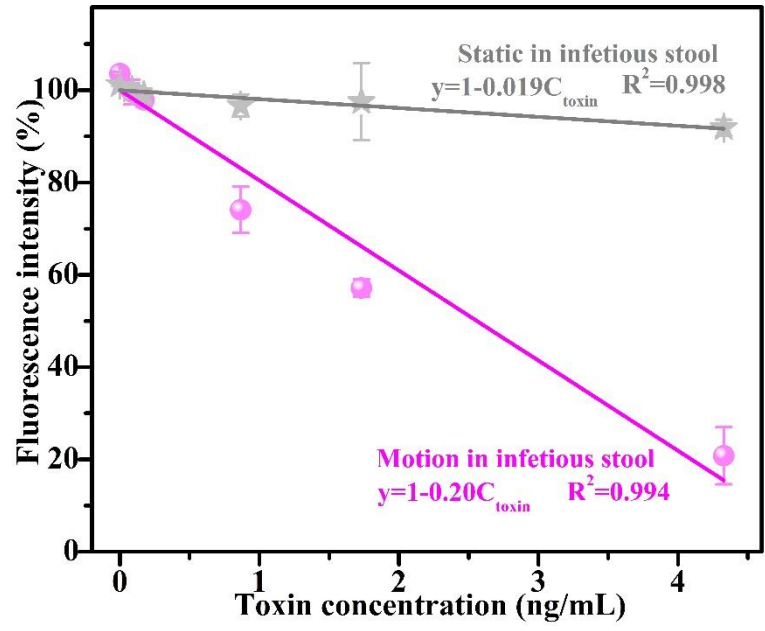


**Fig. S13. Detection calibration curves of the FMSMs.** Fluorescence intensity of the FMSMs navigated for 10 min in toxin-contaminated stool supernatants responding to the toxin concentration and the resultant fitting equation.

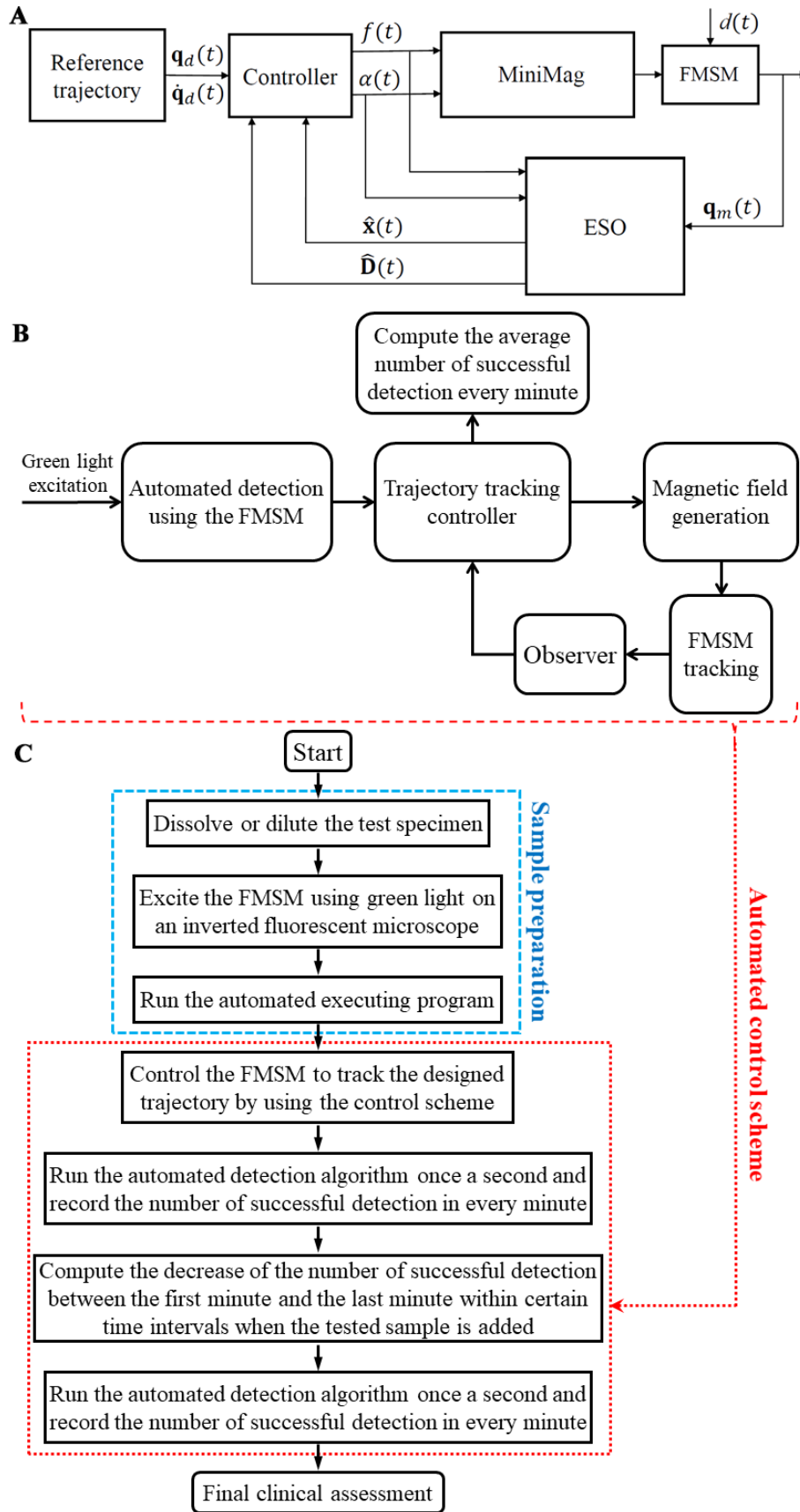


**Fig. S14. Future automated control detection strategy.** (A) Control algorithm, (B) control scheme and (C) flow diagram for automated detecting toxin targets using the

FMSMs-based sensing platform. The desired trajectory of the microrobot, also called reference trajectory, is decided by  $q_d(t)$  and  $\dot{q}_d(t)$  functions, which represent the desired position and velocity, respectively. These functions are preset by users and the tracking performance of the reference trajectory is realized by the following control algorithm

$$\begin{cases} f_x(t) = K_1(q_{d_x}(t) - \hat{q}_x(t)) + \frac{1}{a_0}\dot{q}_{d_x}(t) - \frac{1}{a_0}\hat{D}_x(t) \\ f_y(t) = K_2(q_{d_y}(t) - \hat{q}_y(t)) + \frac{1}{a_0}\dot{q}_{d_y}(t) - \frac{1}{a_0}\hat{D}_y(t) \\ f(t) = \text{sat}(\sqrt{f_x^2(t) + f_y^2(t)}, f_{max}) \\ \alpha(t) = \arctan 2(f_y(t)/f_x(t)) \end{cases}$$

where  $K_i$  ( $i = 1, 2$ ) are positive control gains tuned by discrete-time simulations with the real control frequency, and  $\text{sat}(a, b)$  is a saturation function defined as

$$\text{sat}(\sigma, b) = \begin{cases} \sigma, & \sigma \leq b \\ b, & \sigma > b \end{cases}$$

An extended state observer (ESO) is designed to estimate the velocity and position of the FMSM. The location of the FMSM  $q_m(t)$  is fed back by the fluorescence camera. Moreover, the lumped disturbance  $\hat{D}(t)$  is also estimated. These functions conform to the following equation, where

$$\hat{x}(t) = [\hat{x}_1(t), \hat{x}_2(t), \hat{x}_3(t), \hat{x}_4(t)]^T = [\hat{q}_x(t), \hat{D}_x(t), \hat{q}_y(t), \hat{D}_y(t)]^T$$

is the state estimation vector,  $\beta_i$  ( $i = 1, \dots, 4$ ) are the pertinent constants, and  $\epsilon$  is the constant gain. In the controller, the estimated disturbance is compensated so that the robustness to external disturbance is guaranteed. The controller is also designed to promise the bounded tracking error subject to bounded disturbances

$$\begin{cases} \dot{\hat{x}}_1(t) = \hat{x}_2(t) + a_0 f(t) \cos(\alpha(t)) + \frac{\beta_1}{\epsilon}(q_{xm}(t) - \hat{x}_1(t)) \\ \dot{\hat{x}}_2(t) = \frac{\beta_2}{\epsilon^2}(q_{xm}(t) - \hat{x}_1(t)) \\ \dot{\hat{x}}_3(t) = \hat{x}_4(t) + a_0 f(t) \sin(\alpha(t)) + \frac{\beta_3}{\epsilon}(q_{ym}(t) - \hat{x}_3(t)) \\ \dot{\hat{x}}_4(t) = \frac{\beta_4}{\epsilon^2}(q_{ym}(t) - \hat{x}_3(t)) \end{cases}$$

The identical tracking error of the trajectory, about  $5 \mu\text{m}$ , can be realized. To track the FMSM, we currently use the adaptive mean-shift method which is robust to the fluorescence changing (decay). The fluorescence area of the FMSM is also calculated and recorded in real time via image processing. Utilizing the scheme and algorithm diagram described above, the stability of trajectory following the decaying

fluorescence can be ensured well. For the detailed stability analysis, please refer to our previous report about automated control given by Yang, et al, *IEEE Trans. Nanotech.*

**Table S1. Specific surface areas and pore parameters of the samples.** Original spores, spore@Fe<sub>3</sub>O<sub>4</sub> hybrids and fluorescent magnetic spore-based (spore@Fe<sub>3</sub>O<sub>4</sub>@CDs) microrobots (FMSMs).

Sample	S <sub>BET</sub> (m <sup>2</sup> /g)	V <sub>total</sub> (cm <sup>3</sup> /g)	D <sub>ave</sub> (nm)
Spore	6.74	0.0269	84.38
Spore@Fe <sub>3</sub> O <sub>4</sub>	10.63	0.0131	25.38
Spore@Fe <sub>3</sub> O <sub>4</sub> @CDs	12.96	0.1621	73.16

**Movie S1. Magnetic actuation of the FMSMs using a rotating magnetic field.**

**Movie S2. Swimming of the FMSMs in different media.**

**Movie S3. Fluorescence tracking of the FMSMs in different media.**

**Movie S4. Automated fluorescence signal-based servoing of the FMSMs in predefined trajectories.**

**Movie S5. Fluorescence detection using the FMSMs in clinical stool supernatant.**